Available online at www.sciencedirect.com
ScienceDirect
Journal of Power Sources 174 (2007) 473–479
JOURNAL OF POWER SOURCES
www.elsevier.com/locate/jpowsour

Synthesis and electrochemical properties of lithium non-stoichiometric $Li_{1+x}(Ni_{1/3}Co_{1/3}Mn_{1/3})O_{2+\delta}$ prepared by a spray drying method

Jung-Min Kim, Naoaki Kumagai *, Yoshihiro Kadoma, Hitoshi Yashiro

Department of Frontier Materials and Functional Engineering, Graduate School of Engineering, Iwate University, 4-3-5 Ueda, Morioka, Iwate 020-8551, Japan

Available online 30 June 2007

Abstract

Lithium non-stoichiometric $Li[Li_x(Ni_{1/3}Co_{1/3}Mn_{1/3})_{1-x}]O_2$ materials ($0 \le x \le 0.17$) were synthesized using a spray drying method. The electrochemical properties and structural stabilities of the synthesized materials were investigated. The synthesized materials exhibited a hexagonal structure in all the x-value and the lattice parameters of the materials were gradually decreased with increasing x-value due to an increasing amount of Ni^{3+} ions for charge compensation. The capacity retention ability and rate capability of the stoichiometric $Li(Ni_{1/3}Co_{1/3}Mn_{1/3})O_2$ material were improved by increasing x-value, the so-called overlithiation. We found that the overlithiated materials could keep more structural integrity than the stoichiometric one during electrochemical cyclings, which could be one of reasons for a better electrochemical properties of the overlithiated materials.

Keywords: Battery; Positive electrode; $LiNi_{1/3}Co_{1/3}Mn_{1/3}O_2$; Spray drying; Lithium excess

1. Introduction

Since $Li(Ni_xCo_{1-2x}Mn_x)O_2$ ($0 \le x \le 1/2$) compounds have been introduced as promising positive electrode materials for lithium-ion batteries [1–3], a lot of researches have focused on the layered lithiated ternary transition metal oxide system. Of these, $Li(Ni_{1/2}Mn_{1/2})O_2$ ($x = 1/2$) and $Li(Ni_{1/3}Co_{1/3}Mn_{1/3})O_2$ ($x = 1/3$) materials have been investigated by many researchers because of good electrochemical properties and interesting structural feature [4–8]. However, there is a need to improve their electrochemical performance to meet commercial demand. Recently, several research groups have investigated the substitution of lithium ion for transition metal ions, the so-called overlithiation, to improve electrochemical properties [9,13,16–18,20]. Our research group also investigated the structure of lithium non-stoichiometric $Li[Li_y(Ni_{1/2}Mn_{1/2})_{1-y}]O_2$ material using Neutron diffraction and X-ray absorption near-edge spectroscopy (XANES), and better electrochemical performance and thermal stability were achieved for the overlithiated $Li[Li_{0.06}(Ni_{1/2}Mn_{1/2})_{0.94}]O_2$ material [9]. Recently, we also reported changes in the oxidation states of transition metals and the structure of $LiNi_{1/3}Co_{1/3}Mn_{1/3}O_2$ materials during the first lithium de-intercalation using XANES [5]. In this paper, we prepared the $Li[Li_x(Ni_{1/3}Co_{1/3}Mn_{1/3})_{1-x}]O_2$ materials ($0 \le x \le 0.17$) using a spray drying method and investigated the effect of the overlithiation on the physical and electrochemical properties of $Li[Li_x(Ni_{1/3}Co_{1/3}Mn_{1/3})_{1-x}]O_2$ materials.

2. Experimental

The $Li[Li_x(Ni_{1/3}Co_{1/3}Mn_{1/3})_{1-x}]O_2$ materials were synthesized using a spray drying method. $LiNO_3$ and $Me(CH_3COO)_2{\cdot}4H_2O$ (Me = Ni, Co, and Mn) were used as starting materials to prepare a spray-dried precursor. The molar ratio of Li/(Ni + Co + Mn) in the starting composition was changed to prepare several overlithiated materials with different x-values. The spray-dried precursor was burned out at 400 °C for 6 h in air then pelletized. The pelletized precursor was calcined at 950 °C for 24 h in the limited air atmosphere to synthesize $Li[Li_x(Ni_{1/3}Co_{1/3}Mn_{1/3})_{1-x}]O_2$ ($0 \le x \le 0.17$) materials. The more detail synthetic procedure was described in our previous report [10]. The chemical compositions of the synthesized materials were analyzed by an atomic absorption spectroscopy.

* Corresponding author. Fax: +81 19 621 6328.
E-mail address: nkumagai@iwate-u.ac.jp (N. Kumagai).

0378-7753/$ – see front matter © 2007 Elsevier B.V. All rights reserved.
doi:10.1016/j.jpowsour.2007.06.183

The structure of the synthesized materials were analyzed by X-ray diffractometer (XRD) with Cu Kα radiation. The particle morphologies of the materials were observed using scanning electron microscopy. X-ray photoelectron spectra of the synthesized materials were obtained using PHI 5600 spectrometer (Perkin Elmer) with the monochromatized Al Kα radiation.

For the electrochemical characterization, the synthesized material, acetylene black, and polyvinylidene fluoride (80:10:10, w/w/w) mixed with *N*-methylpyrrolidinon to prepare positive electrode. A 2032 type of coin cell consisted of the positive electrode, lithium metal foil as a negative electrode, and 1 M $LiPF_6$ in ethylene carbonate (EC)–diethylene carbonate (DEC) (1:2, v/v) as an electrolyte. The cell was cycled by a galvanostatic method between 4.5 and 2.8 V *vs*. Li^0 at 25 °C. The structural modifications of the electrochemically cycled materials were observed by *ex situ* XRD.

3. Results and discussion

3.1. Powder characteristics

Fig. 1 shows XRD patterns of the spray-dried precursors burned out at 400 °C for 6 h in air. The burned-out precursors were mainly composed of lithiated transition metal oxides, transition metal oxides, and Li_2CO_3. The portion of Li_2CO_3 increased with increasing Li/Me value (Me = transition metals) in the starting composition. The burned-out precursors were calcined at 950 °C for 24 h in the limited air atmosphere to synthesized $Li[Li_x(Ni_{1/3}Co_{1/3}Mn_{1/3})_{1-x}]O_2$ materials. Fig. 2 shows the XRD results of the synthesized materials. The main intense diffraction peaks could be indexed based on a hexagonal α-$NaFeO_2$ structure. However, small peaks were observed between 20° and 23° in 2θ and the peaks gradually broadened with increasing Li/Me (Fig. 2b). These peaks are probably due to the superlattice ordering of the transition metal ions within transition metal layer as discussed by Ohzuku et al. [11,12] or locally disordered (nano-domain of Li_2MnO_3) structure [8]. The material with $x_{det.} = -0.05$ and 0.17 contained lithiated NiO and Li_2CO_3,

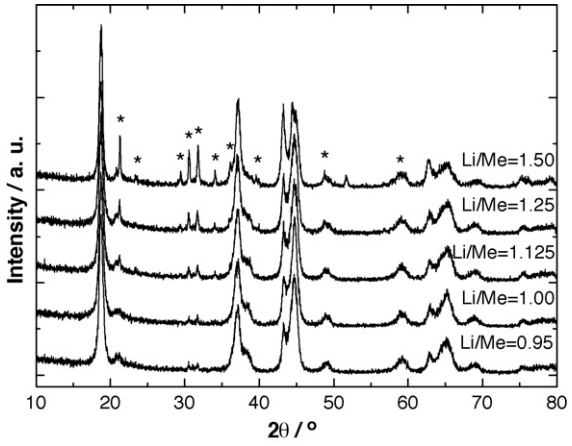

Fig. 1. XRD patterns of the spray-dried precursors burned out at 400 °C for 6 h in air. Li/Me (Me = transition metals) indicates the molar ratio of lithium to transition metals in starting composition. The asterisk represents Li_2CO_3 phase.

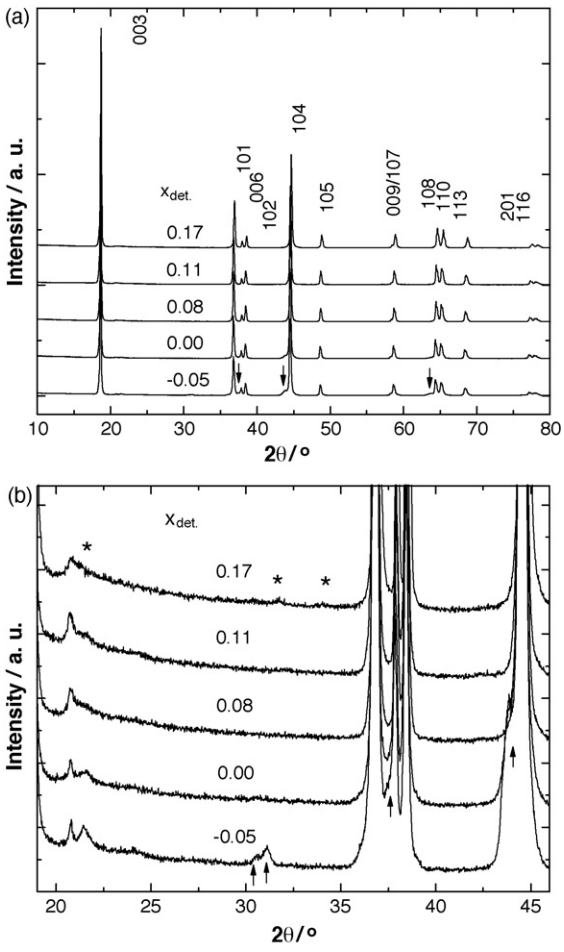

Fig. 2. (a) XRD patterns of $Li[Li_x(Ni_{1/3}Co_{1/3}Mn_{1/3})_{1-x}]O_2$ ($x_{det.} = -0.05$, 0.00, 0.08, 0.11, and 0.17) materials calcined at 950 °C for 24 h in the limited air atmosphere and (b) the enlarged XRD patterns between 19° and 46° in 2θ. The asterisk and the arrow represent Li_2CO_3 and impurity phase, respectively. The $x_{nom.}$ is not the real value of lithium in the material but the assumed value from the Li/Me ratio in the starting composition.

respectively (Fig. 2b). The XRD results indicate that the overlithiation is achieved by the reaction of lithiated transition metal oxides, transition metal oxides, and Li_2CO_3. Therefore, unreacted lithiated NiO and Li_2CO_3 were observed in Li/Me = 0.95 and 1.5, respectively. Thus, the synthesized material was carefully washed with distilled water to remove Li_2CO_3 prior to use as the positive electrode material.

The chemical formula of the synthesized material can be expressed in the layered notation, $(Li_{1+x})_{3b}(Ni_{1/3}Co_{1/3}Mn_{1/3})_{3a}(O_{2+\delta})_{6c}$ (δ is changeable corresponding to the excess lithium). However, the site occupancies of 3b and 6c sites are limited to one and two, respectively, so that the formula should be reconsidered as $Li_{1.00}[Li_x(Ni_{1/3}Co_{1/3}Mn_{1/3})_{1-x}]O_2$, indicating that the transition metals are substituted by lithium. As a result, the increase of average oxidation state of transition metal ions is expected, which was observed in XPS results in Fig. 4. This substitution was also confirmed by Neutron diffraction study in our previous report [13]. To determine the *x*-value in $Li_{1.00}[Li_x(Ni_{1/3}Co_{1/3}Mn_{1/3})_{1-x}]O_2$, elemental analysis was carried out by atomic absorption spectroscopy. As listed in Table 1,

Table 1
Chemical compositions and pellet densities of $Li[Li_x(Ni_{1/3}Co_{1/3}Mn_{1/3})_{1-x}]O_2$ materials calcined at 950 °C for 24 h

Li/Me	Chemical composition	$x_{det.}$	Density[a] ($g\,cm^{-3}$)
0.95	$Li_{0.95}(Ni_{0.33}Co_{0.33}Mn_{0.34})O_2$	−0.05(1)	–
1.00	$Li(Ni_{0.33}Co_{0.34}Mn_{0.33})O_2$	0.00(1)	2.7(1)
1.125	$Li_{1.00}[Li_{0.08}(Ni_{0.33}Co_{0.34}Mn_{0.33})_{0.92}]O_2$	0.08(1)	2.8(1)
1.25	$Li_{1.00}[Li_{0.11}(Ni_{0.33}Co_{0.34}Mn_{0.33})_{0.89}]O_2$	0.11(1)	3.3(2)
1.5	$Li_{1.00}[Li_{0.17}(Ni_{0.32}Co_{0.35}Mn_{0.33})_{0.83}]O_2$	0.17(1)	3.9(2)

[a] The density is not true density but pellet density.

the $x_{det.}$-value in the synthesized materials were found to be −0.05 to 0.17. If lithium ions substitute for transition metal ions, the transition metal ions should be oxidized to compensate the charge balance under the assumption of no oxygen deficiency, probably Ni^{2+} is oxidized to Ni^{3+} because the oxidation of Ni^{2+} is energetically more favorable than those of Co^{3+} and Mn^{4+}. Consequently, the amount of substitutable lithium is limited to $x_{lim.} = 0.143$, corresponding to the chemical formula of $Li_{1.00}[Li_{0.143}(Ni_{1/3}{}^{3+}Co_{1/3}{}^{3+}Mn_{1/3}{}^{4+})_{0.857}]O_2$. However, the $x_{det.}$-values for the material with Li/Me = 1.5 was found to be 0.17 in ICP-MS result. This value beyond the limit might be due to residual Li_2CO_3 after washing as confirmed by XRD in Fig. 2.

Fig. 3 shows SEM images of $Li[Li_x(Ni_{1/3}Co_{1/3}Mn_{1/3})_{1-x}]O_2$ materials. The average particle size was 2 μm. The pellet densities of the sintered materials increased with increasing $x_{det.}$-value as listed in Table 1. The increase in the pellet density could be attributed to Li_2CO_3 phase that can act as a flux medium as reported in ceramic materials [14,15]. It is also considered that the Li_2CO_3 can contribute to the pellet density.

The structural parameters, average oxidation state of transition metals, and theoretical capacity of $Li[Li_x(Ni_{1/3}Co_{1/3}Mn_{1/3})_{1-x}]O_2$ are given in Table 2. The average oxidation state of transition metals and theoretical capacities of the synthesized materials were calculated based on the formula of $Li(Li_xMe_{1-x})O_2$. A continuous decrease in the lattice parameters was observed as increasing $x_{det.}$-value except for the material with $x_{det.} = -0.05$ due to a large portion of impurity phase. The similar phenomenon, a decrease in lattice parameters with increasing excess lithium, has been reported in the overlithiated layered transition material oxides [16–18]. The decrease in the lattice parameters may be caused by the oxidation of Ni^{2+} ($r_{Ni}{}^{2+} = 0.69$ Å) ions to Ni^{3+} ions ($r_{Ni}{}^{3+} = 0.56$ Å). As a result, theoretical capacity based on the electrons-source (the electrochemical oxidation of transition metals are limited up to +4) should be decreased. Note that the mean oxidation sate of transition metals in the materials with $x_{det.} = 0.17$ is restricted to +3.33 due to the limitation of $x_{lim.} = 0.143$.

In order to confirm the oxidation states of transition metals in the synthesized materials, XPS analysis was performed on the $Li[Li_x(Ni_{1/3}Co_{1/3}Mn_{1/3})_{1-x}]O_2$ materials ($x_{det.} = 0.00$ and 0.17). Fig. 4 shows the transition metal $2p_{3/2}$ XPS spectra for both materials. In Fig. 4a and b, the experimental values of binding energies for Co and Mn ions were found to be ∼780 and ∼642 eV in both materials, respectively. These values are very close to those for Co^{3+} (779.5 eV) and Mn^{4+} (642.2 eV) in $LiNi_{1/3}Co_{1/3}Mn_{1/2}O_2$ [19]. As the binding energies corresponding to trivalent and tetravalent cobalt ions cannot be discriminated, the full width at half maximum (FWHM) of the Co $2p_{3/2}$ peak was measured. The obtained FWHM values of both materials were found to be ∼1.9 eV that was close to that of $Li_{1+x}(Ni_{0.425}Mn_{0.425}Co_{0.15})_{1-x}O_2$ (2.2 eV) where all the cobalt ions are in the trivalent state, in contrast with the metallic $Li_{0.6}CoO_2$ (3.7 eV) where the oxidation state of cobalt is +3.4 [20]. Therefore, the oxidation state of Co and Mn ions in both materials are expected as trivalence and tetravalence, respec-

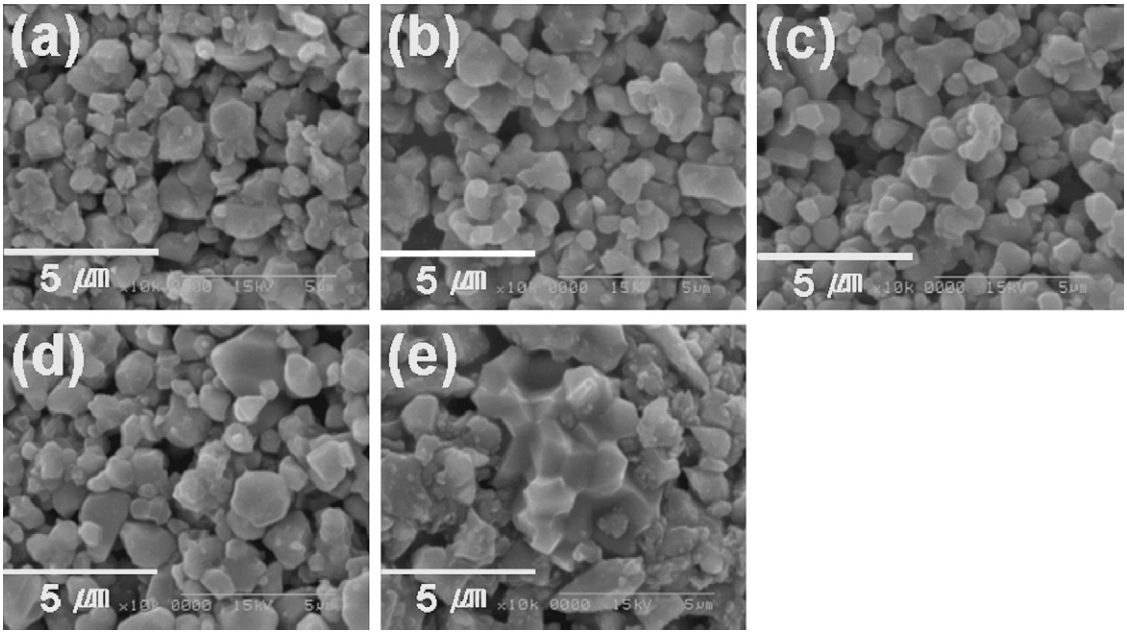

Fig. 3. SEM images of $Li[Li_x(Ni_{1/3}Co_{1/3}Mn_{1/3})_{1-x}]O_2$ materials with $x_{det.}$ = (a) −0.05, (b) 0.00, (c) 0.08, (d) 0.11, and (e) 0.17 calcined at 950 °C for 24 h in air.

Table 2
Structural parameters, average oxidation state of transition metals, and capacities of $Li[Li_x(Ni_{1/3}Co_{1/3}Mn_{1/3})_{1-x}]O_2$ materials

$x_{det.}$	a_{hex} (Å)	C_{hex} (Å)	Oxidation state	Capacity (mAh g^{-1})			
				$Q_{Theo.}$	$Q_{Cha.\ 1st}$	$Q_{Dis.\ 1st}$	$Q_{Irr.}$[a] (1st/2nd/25th)
−0.05	2.8630(9)	14.2599(2)	–	–	176	159	17/2/2
0.00	2.8649(6)	14.2584(1)	3.00	278	189	167	22/3/3
0.08	2.8635(6)	14.2371(3)	3.17	240	205	184	21/3/3
0.11	2.8622(7)	14.2356(2)	3.25	222	210	186	24/3/2
0.17	2.8576(5)	14.2177(2)	3.33	200	226	190	36/7/3

[a] The irreversible capacity loss between charge and discharge capacities at each cycle. The capacities were collected from Fig. 5.

tively. For the Ni $2p_{3/2}$ spectra, two contributions were observed, one at ~854 eV (Ni^{2+}) and another at ~855 eV (Ni^{3+}). The peak of Ni $2p_{3/2}$ spectrum for the material with $x_{det.} = 0.17$ shifted to a higher energy value than that for $x_{det.} = 0.00$, indicating that the portion of Ni^{3+} increased. The XPS analysis confirmed that the overlithiation caused the oxidation of Ni^{2+} ions to Ni^{3+} ions, resulting in decrease in the lattice parameters.

3.1.1. Electrochemical characteristics

Fig. 5 shows voltage *vs.* capacity plots at the 1st, 2nd, and 25th cycle of $Li[Li_x(Ni_{1/3}Co_{1/3}Mn_{1/3})_{1-x}]O_2$. All the cycle curves of the materials showed a S-shaped profile, indicating that no first-order phase transition occurred during cycling between 4.5 and 2.8 V. No significant change in the curve was observed up to the 25th cycle. The theoretical capacities ($Q_{Theo.}$), the obtained charge and discharge capacities at the first cycle ($Q_{Cha.\ 1st}$ and $Q_{Dis.\ 1st}$), and irreversible capacity loss ($Q_{Irr.}$) at the selected cycle are listed in Table 2. A large gap of discharge capacity (*ca.* 20 mAh g^{-1}) between the overlithiated materials ($x_{det.} = 0.08$, 0.11, and 0.17) and the others ($x_{det.} = -0.05$ and 0.00) was observed and the capacity increased as the $x_{det.}$-value increased. The material with $x_{det.} = 0.17$ exhibited the charge capacity of 226 mAh g^{-1} exceeding the theoretical one (200 mAh g^{-1}) and, as a result, a larger $Q_{Irr.}$ of 36 mAh g^{-1} than the others at the 1st cycle. The similar capacity loss at the 1st cycle have been reported in the layered $Li[Li_{1/3-2x/3}Ni_xMn_{2/3-x/3}]O_2$ ($x < 1/2$) caused by the simultaneous extraction of lithium and oxygen ions [21]. Choi et al. reported that the capacity loss of $LiNi_{1/3}Co_{1/3}Mn_{1/3}O_2$ is increased with increasing the surface area, which is related with an irreversible anodic peak around 4.5 V [22]. Although the origin of the irreversible capacity loss at the first cycle in our materials is not verified yet, we assume that the capacity loss in our material may be mainly caused by the side reaction between electrolyte and surface layer of the positive electrode material and additionally the oxygen release. For instance, the first charge capacity of the material with $x_{det.} = 0.17$ is caused by Li^+ extraction until the oxidation states of transition metals reach to +4, then further capacity can be delivered by the way mentioned above. However, the irreversible capacity loss decreased in the 2nd and 25th cycles, indicating that this phenomenon only occurred at the first cycle.

The different cells were cycled up to 50th cycles using the same conditions of Fig. 5. Fig. 6 shows the results of discharge capacities for $Li[Li_x(Ni_{1/3}Co_{1/3}Mn_{1/3})_{1-x}]O_2$ ($x_{det.} = 0.00$, 0.08, 0.11, and 0.17) materials and the inset figure shows capacity retentions in percentage. Although the capacities of these cells

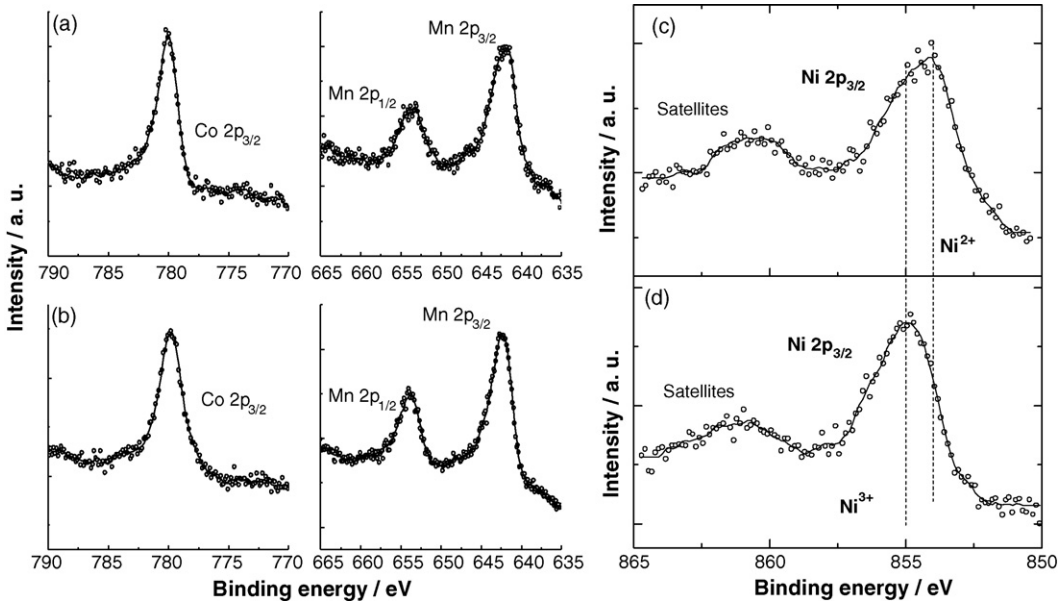

Fig. 4. XPS spectra for Co and Mn ions of $Li[Li_x(Ni_{1/3}Co_{1/3}Mn_{1/3})_{1-x}]O_2$ materials with (a) $x_{det.} = 0.00$ and (b) $x_{det.} = 0.17$, and the Ni XPS spectra for (c) $x_{det.} = 0.00$ and (d) $x_{det.} = 0.17$.

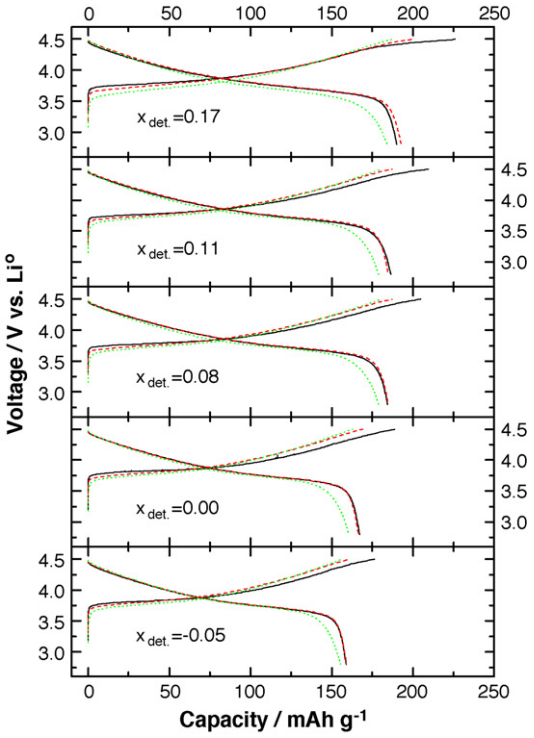

Fig. 5. Voltage *vs.* capacity plots at the 1st (a solid line), 2nd (a dashed line), and 25th cycle (a dotted line) of $Li[Li_x(Ni_{1/3}Co_{1/3}Mn_{1/3})_{1-x}]O_2$ cycled with a constant current density of 30 mA g^{-1} between 4.5 and 2.8 V *vs.* Li^0 at 25 °C.

were higher than those of Fig. 5, both cases showed a same cycle curve. The discharge capacity of these cells also increased with increasing $x_{det.}$-value. The overlithiated material with $x_{det.} = 0.17$ could deliver a high discharge capacity of 209 mAh g^{-1} at the first cycle, while the stoichiometric one showed 183 mAh g^{-1}. At the 50th cycle, the overlithiated materials kept 86% of their initial capacity, whereas the stoichiometric one retained 77%. Although the overlithiation led to a decrease in theoretical capacity and a large irreversible capacity at the first cycle, it can improve capacity retention ability and reversible capacity when the materials were cycled at high voltage region.

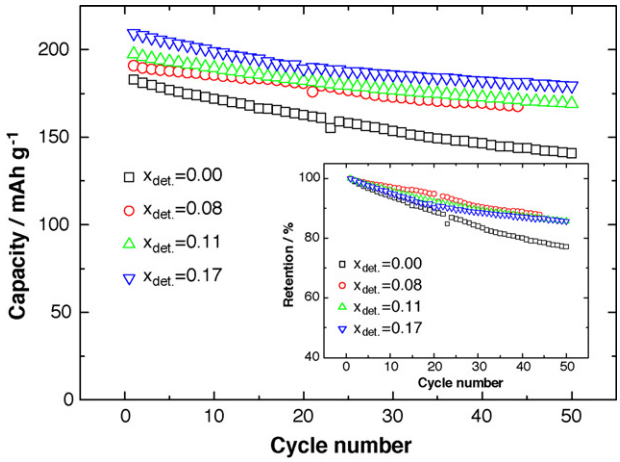

Fig. 6. (a) Discharge capacities of the $Li[Li_x(Ni_{1/3}Co_{1/3}Mn_{1/3})_{1-x}]O_2$ materials ($x_{det.} = 0.00$, 0.08, 0.11 and 0.17) as a function of cycle number and inset figure showed the retentions of discharge capacities for the materials. The synthesized materials were cycled between 4.5 and 2.8 V *vs.* Li^0 with 30 mA g^{-1} at 25 °C.

3.2. Structural stability of Li^+ extracted and re-inserted materials

The structural modifications of $Li[Li_x(Ni_{1/3}Co_{1/3}Mn_{1/3})_{1-x}]O_2$ ($x_{det.} = 0.00$, 0.11, and 0.17) materials were monitored by XRD during lithium de-/intercalation processes. For the XRD measurement, the synthesized materials were charged with *ca.* 1/100 C rate. The extracted or re-inserted Li^+ moles were estimated based on the obtained capacities and a possible error of the *y*-value is in ±0.02. Fig. 7 shows the initial charge curves for $Li[Li_x(Ni_{1/3}Co_{1/3}Mn_{1/3})_{1-x}]O_2$ ($x_{det.} = 0.00$, 0.11, and 0.17) materials and the corresponding XRD patterns with the step of 0.1 M lithium extraction. As increasing *y*-value, (0 0 *l*) peaks shifted to a low angle due to the repulsion energy between adjacent oxygen atoms, and then returned to a high angle at the highly lithium extracted state, while (1 0 8) and (1 1 0) peaks gradually separated each other with lithium extraction. All the three materials showed a similar change of Bragg's peak posi-

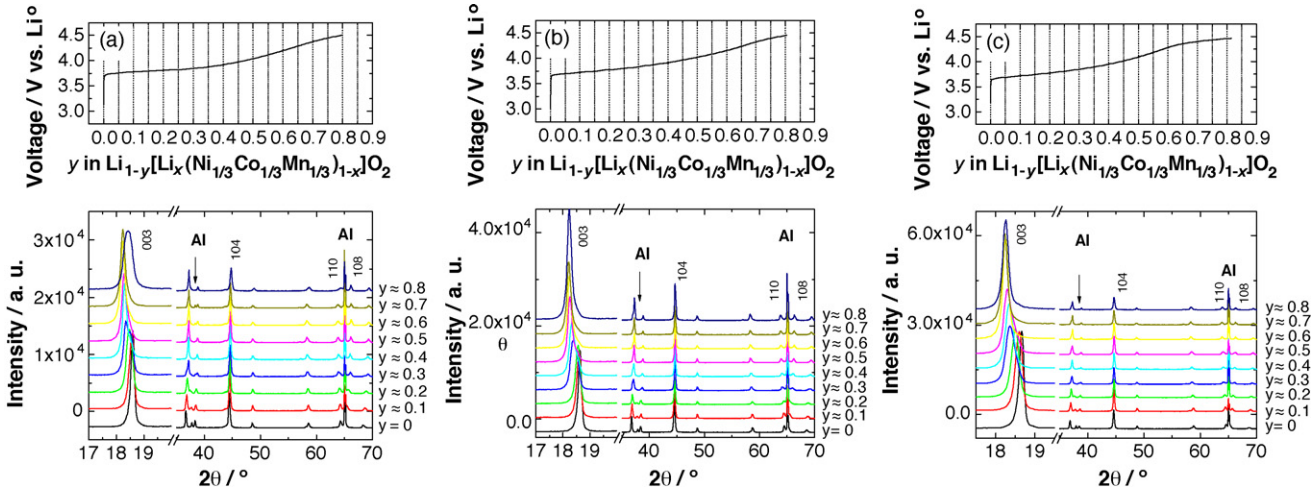

Fig. 7. The initial charge curve and *ex situ* XRD patterns of $Li[Li_x(Ni_{1/3}Co_{1/3}Mn_{1/3})_{1-x}]O_2$ material with $x_{det.}$ = (a) 0.00, (b) 0.11, and (c) 0.17. The extracted Li^+ mole was estimated based on the obtained capacity and a possible error of the *y*-value is in ±0.02.

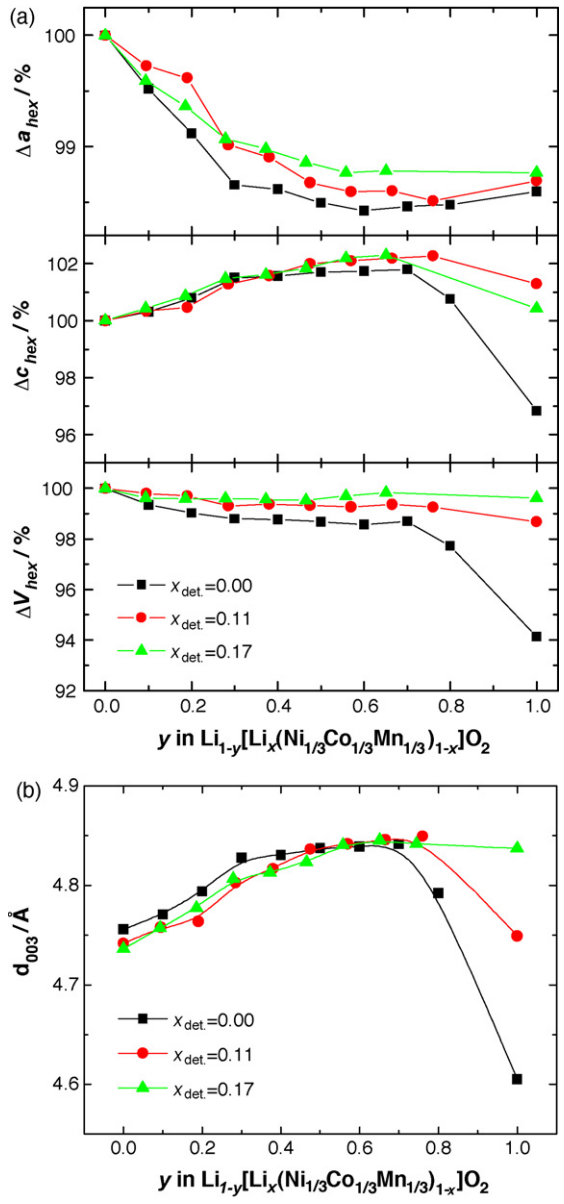

Fig. 8. The variations in the hexagonal lattice parameters (a_{hex} and c_{hex}) and unit cell volume for $Li_{1-y}[Li_x(Ni_{1/3}Co_{1/3}Mn_{1/3})_{1-x}]O_2$ materials ($x_{det.} = 0.00$, 0.11, and 0.17) during the initial charge. The y-values in $Li_{1-y}[Li_x(Ni_{1/3}Co_{1/3}Mn_{1/3})_{1-x}]O_2$ were estimated based on the charge capacities, and a possible error of the y value is in ±0.02.

tion with lithium extraction. No new phase was observed till the end of charge, indicating that the structure is preserved during lithium extraction, that is, a single-phase reaction seems to occur during lithium extraction up to $y \approx 0.8$. At the end of charge state, however, the stoichiometric material ($x_{det.} = 0.00$) showed a severe peak broadening of (0 0 3) ($FWHM_{003} = 0.38°$) compared with those of the overlithiated materials (0.18° and 0.17° for $x_{det.} = 0.11$ and 0.17, respectively).

Fig. 8 shows the changes in the lattice parameters of the synthesized materials during the first electrochemical lithium extraction. The overlithiated materials showed 2% change in the unit cell volume, whereas the stoichiometric one exhibited 6%. The volume change of these materials corresponded with the variation of c_{hex}. As can be seen in Fig. 8b, the values for d_{003} (the slab distance between MO_6 slabs; M = transition metal) gradually increased until y reached 0.7 in all the materials due to the oxygen–oxygen interaction across the van der Waals gab. After that value, the d_{003} showed different behaviors with the material. The d_{003} for the stoichiometric one dramatically decreased from 4.83 to 4.6 Å at the end of charge state, indicating that a covalent characteristic became predominant over an ionic one by lithium extraction as $Li_xNi_{1.02}O_2$ ($x \leqq 0.3$) [23]. On the other hand, the overlithiated material with $x_{det.} = 0.11$ and 0.17 showed a small contraction and little shrinkage of d_{003} at the end of charge state, respectively. These results suggest that an ionic character may be dominant over a covalent one in the overlithiated materials at the deeply charged state due to the existence of lithium ions in the transition metal site, resulting in small volume change during charge process. Therefore, we think that the structural stability of the overlithiated materials at deeply charged state can contribute to good electrochemical performance.

Fig. 9 shows *ex situ* XRD patterns of the $Li_{1-y}[Li_x(Ni_{1/3}Co_{1/3}Mn_{1/3})_{1-x}]O_2$ materials ($x_{det.} = 0.00$, 0.11, and 0.17) at the fully charged and discharged states with the XRD patterns of pristine materials for comparison. At the 1st fully charged sate, the stoichiometric material ($x_{det.} = 0.00$) showed a significant (0 0 3) peak broadening and a new peak at 19.32° in 2θ ($d = ca.$ 4.59 Å) emerged (Fig. 9a), while the overlithiated materials ($x_{det.} = 0.11$ and 0.17) retained their initial structure with a broad (0 0 3) peak (Fig. 9b and c). At the 1st fully discharged state, all the materials returned to their initial structure, indicating that electrochemical lithium extraction and insertion are

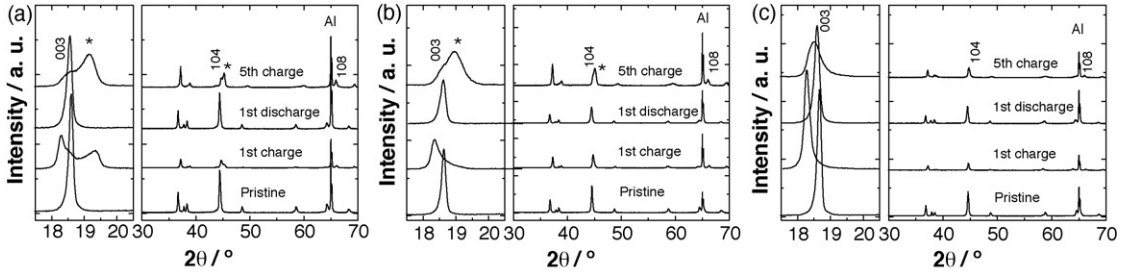

Fig. 9. *Ex situ* XRD patterns of the pristine, 1st charged, 1st discharged, and 5th charged states for $Li[Li_x(Ni_{1/3}Co_{1/3}Mn_{1/3})_{1-x}]O_2$ materials with $x_{det.}$ = (a) 0.00, (b) 0.11, and (c) 0.17. The materials were cycled using CC – CV (constant current – constant voltage) mode with *ca.* 1/100 C rate until the capacity reached to the theoretical one. Al in the XRD patterns indicated an aluminum foil current collector which was used as an internal standard for calibration. The new peaks are marked by the asterisk.

reversible. At the 5th charged state, the new peak (19.32°) intensified in the stoichiometric material ($x_{det.} = 0.00$) and the similar peak was observed in the overlithiated material with $x_{det.} = 0.11$. However, the overlithiated material with $x_{det.} = 0.17$ showed no new peak but showed more broad (0 0 3) than that of 1st fully charged state.

4. Conclusion

The $Li[Li_x(Ni_{1/3}Co_{1/3}Mn_{1/3})_{1-x}]O_2$ ($0 \leq x \leq 0.17$) materials were synthesized using a spray drying method. The overlithiation of these materials gave rise to a decrease in hexagonal lattice parameters due mainly to the oxidation of Ni^{2+} ions to Ni^{3+} ions for charge compensation. It was found that the overlithiated materials showed better electrochemical properties than those of stoichiometric one when the materials were cycled at a high voltage region of 2.8–4.5 V *vs.* Li^0. We believe that better electrochemical properties of the overlithiated materials are due to smaller change in the lattice parameters and more structural stability than those of the stoichiometric one during electrochemical cycling. Our results indicate that the overlithiated $Li[Li_x(Ni_{1/3}Co_{1/3}Mn_{1/3})_{1-x}]O_2$ can be considered as a promising positive electrode material for lithium-ion batteries. However, it should be also examined the thermal stability at charged state and electrochemical properties at high or low temperature prior to commercial use.

Acknowledgements

The authors would like to thank to Ms. Yuko Mitobe and Ms. Aiko Ueyama of Iwate University for their helpful assistance in the experimental work.

References

[1] Z. Lu, D.D. MacNeil, J.R. Dahn, Electrochem. Solid State Lett. 4 (2001) A200.
[2] T. Ohzuku, Y. Makimura, Chem. Lett. (2001) 642.
[3] T. Ohzuku, Y. Makimura, Chem. Lett. (2001) 744.
[4] K.M. Shaju, G.V. Subba Rao, B.V.R. Chowdari, Electrochim. Acta 48 (2003) 1505.
[5] J.-M. Kim, H.-T. Chung, Electrochim. Acta 49 (2004) 937.
[6] A. Van der Ven, G. Ceder, Electrochem. Commun. 6 (2004) 1045.
[7] Y.W. Tsai, B.J. Hwang, G. Ceder, H.S. Sheu, D.G. Liu, J.F. Lee, Chem. Mater. 17 (2005) 3191.
[8] L.S. Cahill, S.-C. Yin, A. Samoson, I. Heinmaa, L.F. Nazar, G.R. Goward, Chem. Mater. 17 (2005) 6560.
[9] S.-T. Myung, S. Komaba, K. Kurihara, K. Hosoya, N. Kumagai, Y.-K. Sun, I. Nakai, M. Yonemura, T. Kamiyama, Chem. Mater. 18 (2006) 1658.
[10] J.-M. Kim, N. Kumagai, H.-T. Chung, Electrochem. Solid State Lett. 9 (2006) A494.
[11] Y. Koyama, N. Yabuuchi, I. Tanaka, H. Adachi, T. Ohzuku, J. Electrochem. Soc. 151 (2004) A1545.
[12] N. Yabuuchi, Y. Koyama, N. Nakayama, T. Ohzuku, J. Electrochem Soc. 152 (2005) A1434.
[13] J.-M. Kim, H.-T. Chung, Electrochim. Acta 49 (2004) 3573.
[14] Q. Li, J. Qi, Y. Wang, Z. Gui, L. Li, J. Eur. Ceram. Soc. 21 (2001) 2217.
[15] M.J. Laurent, G. Desgardin, B. Raveau, J. Mater. Sci. 25 (1990) 599.
[16] Y. Marinov Todorov, K. Numata, Electrochim. Acta 50 (2004) 495.
[17] J. Choi, A. Manthiram, Electrochem. Solid State Lett. 7 (2004) A365.
[18] S. Choi, O.A. Shlyakhtin, J. Kim, Y. Yoon, J. Power Sources 140 (2005) 355.
[19] K.M. Shaju, G.V. Subba Rao, B.V.R. Chowdari, Electrochim. Acta 48 (2002) 145.
[20] N. Tran, L. Croguennec, C. Labrugere, C. Jordy, Ph. Bieesan, C. Delmas, J. Electrochem. Soc. 153 (2006) A261.
[21] Z. Lu, J.R. Dahn, J. Electrochem. Soc. 149 (2002) A815.
[22] J. Choi, A. Manthiram, Electrochem. Solid State Lett. 8 (2005) C105.
[23] L. Croguennec, C. Pouillerie, A.N. Mansour, C. Delmas, J. Mater. Chem. 11 (2001) 131.